ORIGINAL ARTICLE

Mechanical property characterization of mudstone based on nanoindentation technique combined with upscaling method

Qingsong Zhang[1,2] · Zhibin Liu[1,2] · Yasen Tang[3] · Yongfeng Deng[1,2] · Tingyi Luo[3] · Yuting Wang[1,2]

Abstract

The poor mechanical property of mudstone seriously affects the stability of various engineering buildings. For weathered mudstone, the mechanical parameters are difficult to obtain accurately by conventional mechanical experimental methods. In addition, these macroscopic measurements cannot distinguish the mechanical response of different mineral compositions. In this study, the nanoindentation test and the data analysis method of deconvolution were used to systematically evaluate the mechanical properties of various mineral compositions in mudstone at the mesoscale. Then, three upscaling models including Mori–Tanaka (MT), Kuster–Toksöz (KT), and differential effective medium (DEM) were used to obtain the macroscopic mechanical properties. The results show that mudstone can be considered as a highly heterogeneous material with multiple mineral compositions. Among them, illite and various pores constitute the clay matrix, and quartz and feldspar minerals constitute the grain skeleton. The mechanical response of mineral compositions in the interface region was complex, mainly reflecting the composite mechanical properties of clay matrix and various clastic minerals. This characteristic made the overall mechanical properties of the mudstone show good continuity in the nanoindentation test. The Young's moduli (E_{IT}) of the clay matrix, feldspar mineral and quartz in the mudstone were 16.1, 64.84 and 149.69 GPa respectively. The E_{IT} of the mudstone obtained by the three upscaling models was higher than the measured macroscopic values. The model can be effectively optimized by setting the E_{IT} of interfaces to the value of clay matrix.

Keywords Mechanical property · Mudstone · Nanoindentation · Deconvolution · Upscaling models

✉ Zhibin Liu
seulzb@seu.edu.cn

Qingsong Zhang
zqs1019@seu.edu.cn

Yasen Tang
tangyasen@163.com

Yongfeng Deng
noden@seu.edu.cn

Tingyi Luo
luoty0116@163.com

Yuting Wang
220203412@seu.edu.cn

[1] Institute of Geotechnical Engineering, Southeast University, Nanjing 211189, China

[2] National Demonstration Center for Experimental Road and Traffic Engineering Education, Southeast University, Nanjing 211189, China

[3] Guangxi Beitou Highway Construction and Investment Group Co., Ltd., Nanning 530028, China

Introduction

Mudstone has the characteristics of low strength, easy weathering, easy disintegration and softening when exposed to water. In addition, it is widely distributed. For example, in China, the red mudstone is abundantly distributed in Sichuan basin and the junction of Sichuan-Guizhou and Yunnan-Guizhou, with a total area of 826,300 km². Widespread distribution of mudstone has already had a serious impact on the stability of various engineering constructions, such as tunnels (Corkum and Martin 2007; Perras et al. 2015) and highway slopes (Kong et al. 2018; Zhang et al. 2018a, b). Therefore, it is important to systematically analyze and characterize the mechanical properties of mudstone. Uni/triaxial tests of mudstone at the macro scale can obtain mechanical parameters such as elastic modulus and Poisson's ratio. However, for the weathered mudstone, it is more difficult to coring and sample it. Because the mudstone has a high content of clay minerals, and after weathering, the water sensitivity of the rock is enhanced and its cementing

ability is weakened (Kang et al. 2017). During the process of sample preparation, the collected mudstone needs to be cut twice, which is easy to cause secondary damage to the sample and ultimately affect the test results. In addition, these macro testing methods usually treat the rock as a homogeneous material and therefore cannot distinguish between mechanical responses with different mechanical properties and mineral compositions. Therefore, it is necessary to find an alternative method for evaluating the mechanical properties of mudstone.

Nanoindentation provided a new approach to solving the above problems. In recent years, with the development of instrumented indentation micro/nano mechanical testing techniques, nanoindentation testing was gradually being applied to shale, sandstone and coal and other rock materials for characterization of mechanical parameters (Ma et al. 2020). The nanoindentation testing process could be simplified as the process in which the indenter pressed into relevant materials and caused relevant elastoplastic deformation. Various deformation parameters of materials and loads applied by the indenter during the test were also recorded. For example, the hardness (H_{IT}) and E_{IT} of the material can be obtained by the method of Oliver and Pharr method (Oliver and Pharr 2011). For heterogeneous composites, it is difficult to accurately determine which mineral components the indentation acts on. To solve this problem, Constantinides et al. (2006) assumed that the obtained dataset satisfied the Gaussian distribution. Each dataset corresponded to one phase integrals in the composite material. Sun et al. (2021) proposed a targeted nanoindentation technique. The location of each mineral component in the rock was first determined by SEM–EDS, followed by indentation tests at specific locations to obtain the mechanical parameters of the composition. Even more convenient was the use of various statistical methods for processing the results obtained from nanoindentation test. In fact, deconvolution methods have been used for data analysis in previous studies, such as probability density function (PDF) (Zhu et al. 2007), cumulative distribution function (CDF) (Miller et al. 2007), and mixture Gaussian model (Davydov et al., 2011). Deconvolution based on PDF was more intuitive than other statistical methods and was therefore widely used (Du et al. 2022). Nanoindentation is essentially the determination of the fine mechanical properties of material compositions at the micro/nano scale. For rock materials, nanoindentation generally determines the mechanical properties of the mineral composition. In order to establish a connection between the meso- and macro-mechanical properties of rocks, it is often necessary to scale up the meso-mechanical properties of the individual mineral compositions. Representative scale-up models included MT (Mori and Tanaka 1973), KT (Kuster

and Toksöz, 1974), and DEM (Berryman 1992) methods. The rock mechanical parameters obtained by this method can reflect the test results at the macro scale to a certain extent. However, there is often a certain error between the values obtained by the upscaling method and the actual laboratory test results (Hu et al. 2013). Therefore, it has become an urgent problem to propose an effective correction method based on the upscaling model. Mudstone can be seen as a non-homogeneous, multi-phase composite material. Using nanoindentation can obtain the meso-mechanical properties of various mineral fractions and further evaluate the macroscopic mechanical properties of mudstones using a scale-up approach. This technique avoids the disadvantage of difficult sampling and preparation of weathered mudstone, and provides an alternative idea for evaluating the macroscopic mechanical properties of mudstone at the mesoscale.

In this paper, a cross-scale analysis of the meso and macro-mechanical properties of mudstone was carried out in combination with nano-indentation technology and upscaling model. Mudstone in southern Guangxi Zhuang Autonomous Region, China was taken as the research object, the distribution of the overall E_{IT} of mudstone and the relationship between E_{IT} and H_{IT} were obtained by nanoindentation test. The mechanical properties of each mineral composition were also quantified by deconvolution method. Then, the homogenization method of scaling up was used to evaluate the macroscopic mechanical properties of mudstone. Finally, an optimization method based on the scaling model was proposed, which further reduced the error between the mudstone mechanical parameters obtained by upscaling model and the laboratory test results.

Materials

Sampling site

The mudstone chosen for this project came from the side slopes of the S210 provincial highway in southern Guangxi Zhuang Autonomous Region, China. The mudstone slopes were stratified by the Cretaceous (K), Tertiary (E) and Quaternary Holocene (Q4), and the mudstone in the section sampled was mainly from the Cretaceous Dapo Formation (K1d). The specific stratigraphic distribution is shown in Fig. 1b. The mudstone at the sampling point was mainly distributed in the area with a depth of 3.5 m–6.5 m, and the surface was mostly covered with soft silt. The macroscopic characteristics of the site slope are shown in Fig. 1c. There were many weak interlayers at the junction of the mudstone and the sandstone above it, which provided objective material conditions for the occurrence of geological disasters.
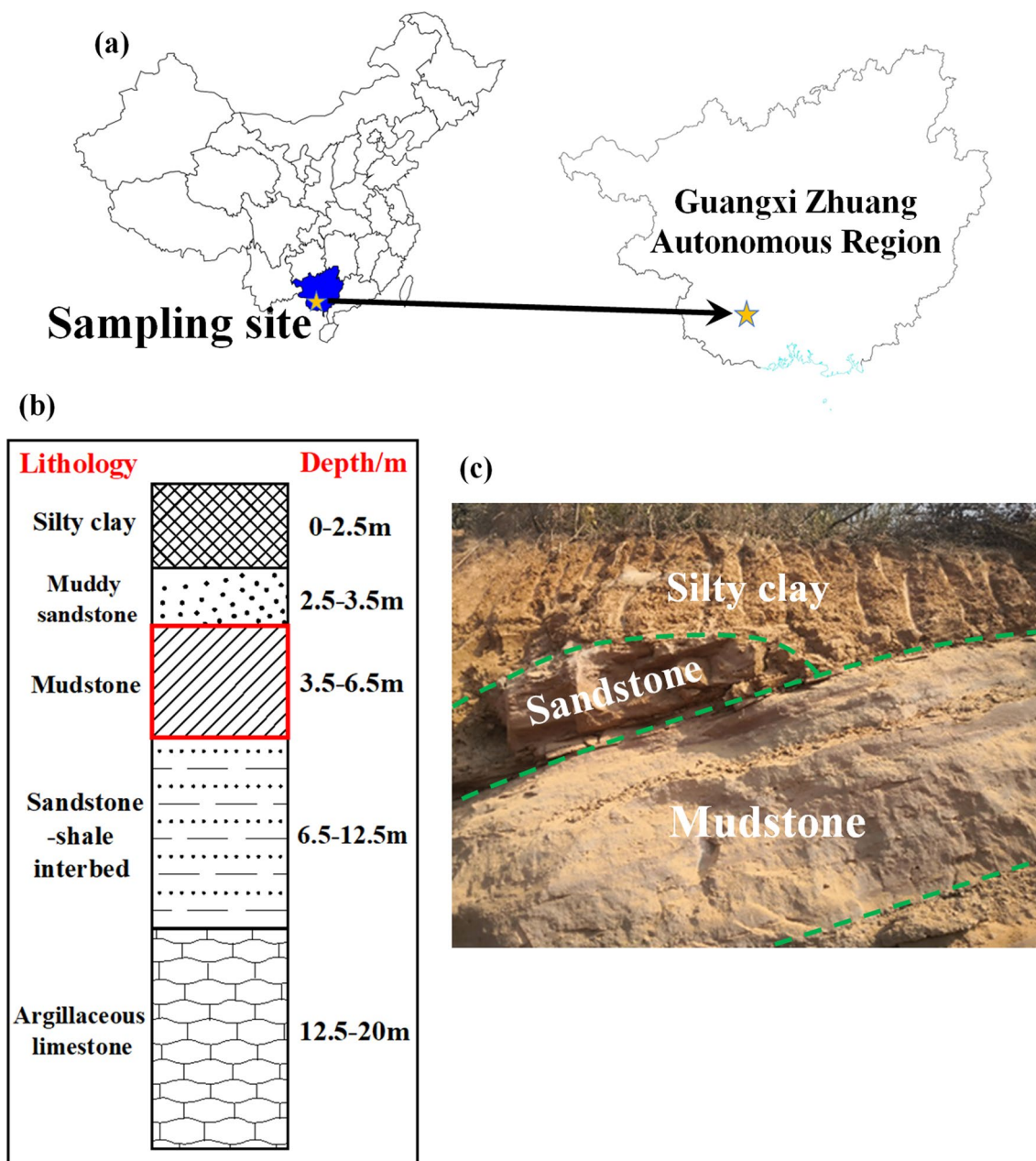
Fig. 1 Basic information on the mudstone at the sampling site, **a** location of the sampling site, **b** stratigraphic distribution of the sampling site **c** photo of the sampling site

Mineral composition of the mudstone

In order to quantitatively analyze the mineral components contained in the mudstone, the Smartlab (3) X-ray diffractometer (produced by Rigaku Corporation) was used to finely scan the sample. For the quantitative analysis of the XRD results, the open-source program Profex was used in combination with the "Rietveld refinement method" (Doebelin and Kleeberg 2015) to obtain the specific content of each composition. The diffraction spectrum of the powder and the results of quantitative analysis are shown in Fig. 2 and Table 1. The main mineral compositions in the mudstone can be divided into three groups: quartz (53.8%), illite (29.9%), and feldspar minerals (16.3% in total). The feldspar minerals included both microcline and albite.

Surface characteristics of the mudstone

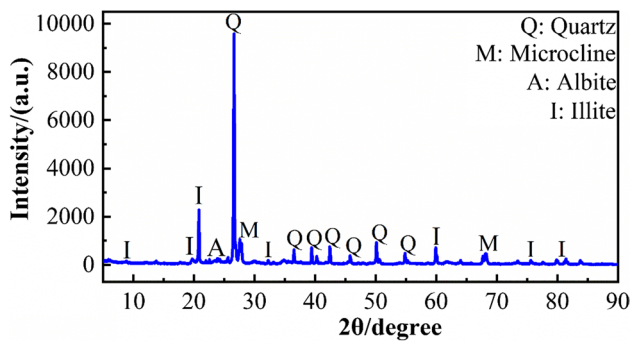Figure 3a is an image of the front side of the mudstone sample magnified 150 times. The main components of

Fig. 2 XRD pattern of mudstone sample

Table 1 Table of mineral compositions of mudstone

Mineral name	Quartz	Microcline	Albite	Illite
Chemical formula	SiO_2	$K(AlSi_3O_8)$	$Na(AlSi_3O_8)$	$K(Al_4Si_2O_9(OH)_3)$
Mass fraction (%)	53.8	13.5	2.8	29.9

these skeletal particles were quartz and feldspar, with clay minerals filling the pores between the skeletal particles and a large number of quartz minerals being wrapped by clay minerals. The fractures on the surface of the mudstone were mostly distributed along the intergrain and were interconnected to a certain extent. Most of these interconnected cracks were less than 5 μm in width, but hundreds of microns in length. Clay minerals mainly composed of illite were in the form of lumps and strands. Part of the illite formed a thin layer in a continuous, non-directional arrangement, which was distributed in the pores between the particles and plays the role of connecting the skeletons of the particles.

Figure 3 shows the distribution of the three elements Si K Al on the mudstone surface. The result of the XRD test shown that element Si was common to all four mineral compositions, so Si was also the most widely distributed. The enrichment degree of Si element in the grain site was significantly higher than that in other regions, because quartz and feldspar minerals together constituted the framework of mudstone. The enrichment degree of K element was low, mainly because only illite and microcline contained potassium element in mudstone, and the proportion was small,

Fig. 3 SEM and EDS mapping of mudstone
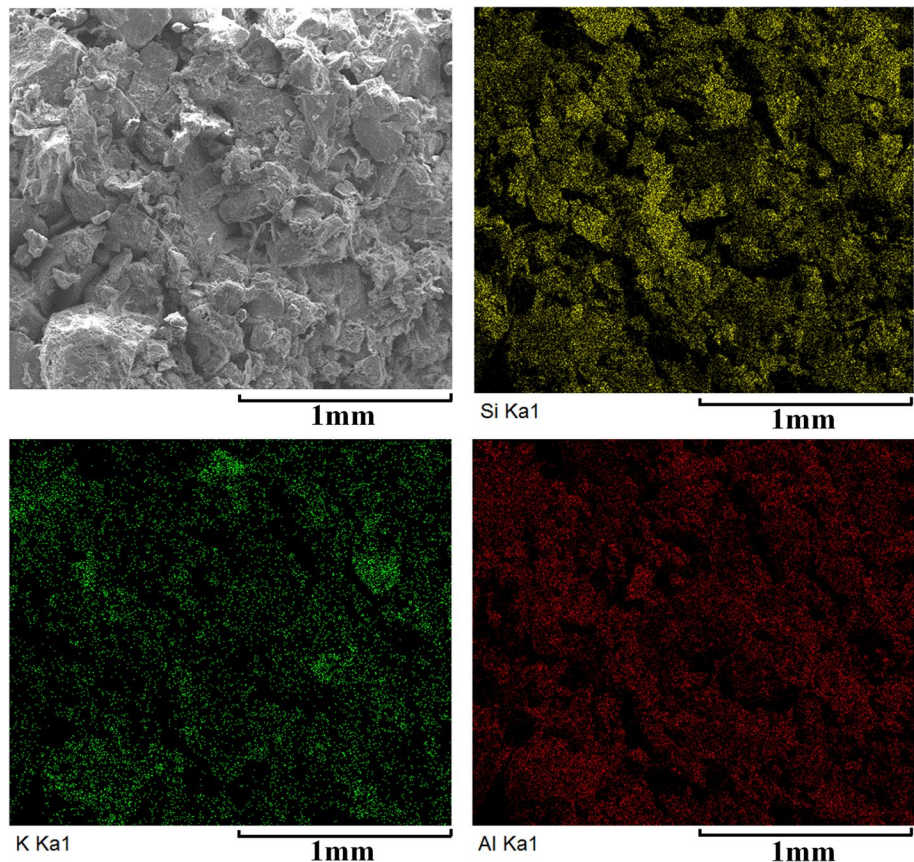
and it was mainly distributed among the particles. The source of Al element was two kinds of feldspar minerals and illite, so it can be seen that its enrichment area was wide, but the enrichment degree was not high. The illite and various pores and crack areas in the mudstone can be collectively referred to as clay matrix (Sun et al. 2020).

Methodology

Nanoindentation test

The nanoindentation tests on the mudstone samples were based on the System 1 nanoindentation mechanical test system (produced by Micro Materials Inc.). The test system was equipped with a Berkovich indenter and can apply loads of 0–500 mN. Before the official start of the nanoindentation test, in order to overcome the influence of uneven structures such as cracks and pores on the original sample surface on the test results, the mudstone samples needed to be pretreated. The mudstone samples were first cut to obtain cubic blocks with 15 mm sides and fixed by wrapping them with a low viscosity epoxy resin. The surface of the cube was then sanded and polished using 800, 1 200, 1 500, 2 000, 2 500 and 3000 grit sandpaper and oil-based diamond polishing solutions with particle sizes of 3.0, 1.0 and 0.5 µm respectively. The surface roughness of the sample after the above treatment can reach the nanometer level below 100 nm (Miller et al. 2007). In order to obtain sufficient data for statistical analysis, 4 indentation matrices were randomly selected on the polished surface of a single sample, each matrix consisted of a 5*5 grid (Fig. 4), and a total of 100 indentation measurements were performed. When carrying out the loading-holding-unloading test, it is necessary to consider the time required to apply the load and ensure that the indentation has a certain depth. In this test, the peak load was set to 3mN. Based on the previous nanoindentation test results of Guangxi mudstone (Luo et al. 2022) and the

size of mineral compositions in the mudstone (Sun et al., 2020), it can be concluded that setting 3 mN as the peak load can effectively control the elastic–plastic deformation of the indentation in the vertical direction within the range of a single mineral composition.

The strain rate was constant during loading and unloading, and the load was held for 10 s after loading was completed. The 10 s holding time was mainly to minimize the creep effect on the elastic unloading (Němeček 2009). Most of the creep deformation of the mudstone take place in the first 5 s (Sun et al. 2021). Therefore, a holding time of 10 s is sufficient for the mudstone material. The entire loading project lasts 70 s.

The raw data obtained from the nanoindentation test actually reflect the relationship between the indentation load and the deformation of the material (Fig. 5a), and a corresponding load–displacement curve is obtained (Fig. 5b) (Wu et al. 2022). By analyzing the parameters of these curves, mechanical parameters such as H_{IT} and modulus of elasticity of the material can be obtained, and the classical data interpretation model proposed by Oliver and Pharr is now widely used (Oliver and Pharr 2004, 1992).

Assuming that the maximum load applied to the material by the indenter is F_{max}, A_c is the projected contact area.
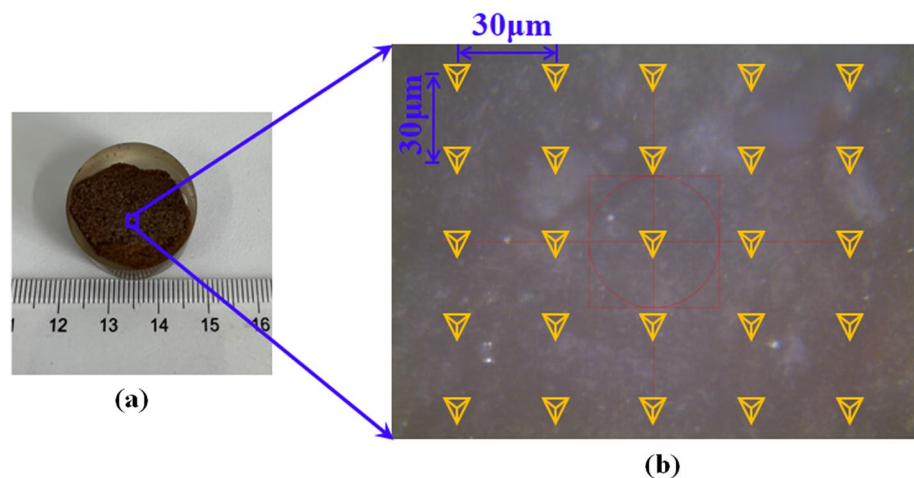
$$A_c = 24.56 h_c^2 \tag{1}$$

The contact depth h_c can be obtained using the load–displacement results:

$$h_c = h - \varepsilon \frac{F}{S} \tag{2}$$

In Eq. 2, ε is a constant related to the geometry of the indenter, dimensionless, and for the Berkovich indenter, $\varepsilon = 0.75$; S is the contact stiffness, mN/µm. The tip radius of the Berkovich indenter is 40 nm (Li et al. 2018).

Fig. 4 Distribution of indentation points

(a)

(b)

(a)

F_{max}

Z

A_C

h_{max} h_c

Mudstone

(b)

Representative normal curve

Holding
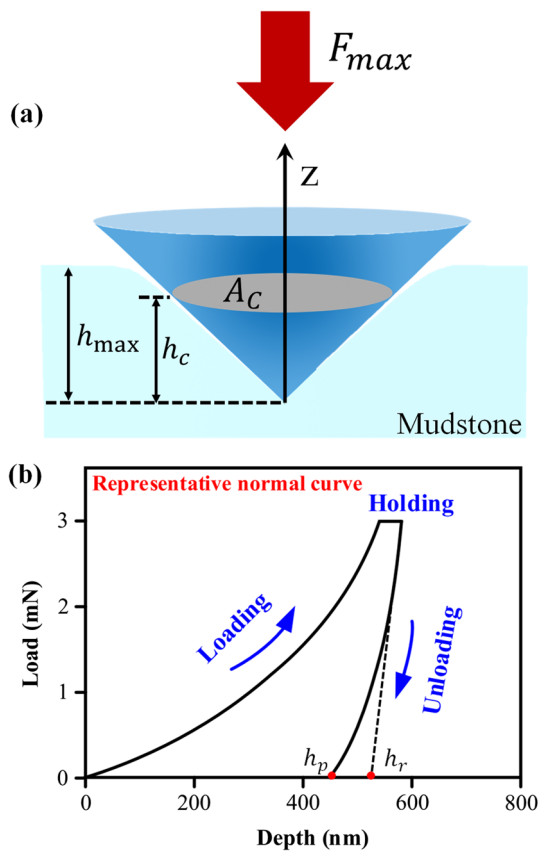
Loading

Unloading

h_p h_r

Fig. 5 Nanoindentation testing technique. **a** Indenter; **b** Typical load-depth curve

The indentation hardness H_{IT} can be calculated according to the following equation:

$$H_{IT} = \frac{F_{max}}{A_c} \tag{3}$$

E_{IT} is the Young's modulus at the indentation, where the converted modulus is E_r, which can reflect the composite elastic deformation of the indenter and the sample. The E_{IT} of the mudstone can also be calculated from the converted modulus of elasticity, which is given by:

$$E_r = \frac{\sqrt{\pi} \cdot S}{2 \cdot \beta \sqrt{A_c}} \tag{4}$$

The equation for calculating the plane strain elastic modulus $E*$ is:

$$E^* = \frac{1}{\frac{1}{E_r} - \frac{1 - v_i^2}{E_i}} \tag{5}$$

The E_{IT} at the indentation is:

$$E_{IT} = E^* \cdot \left(1 - v_s^2\right) \tag{6}$$

The Poisson's ratio of typical mudstone is $v_s = 0.18 \sim 0.35$, which was taken as $v_s = 0.3$ in this study. In the equation: β is a geometric factor related to the shape of the indenter. E_i is the indenter elastic modulus (diamond elastic modulus is 1141 GPa); v_i is the indenter Poisson's ratio (diamond Poisson's ratio is 0.07) (Oliver and Pharr 1992).

Statistical methods for nanoindentation test results

For mudstone, the difficulty in using nanoindentation technology is that it is difficult to select a specific material for indentation and repeat the test. To address this challenge, it is possible to treat each indentation test as an independent random event and apply statistical techniques to analyze the results (Ulm et al 2007). The mechanical properties of individual constituent phases can be extracted by deconvolution of a large number of indentation statistics (Hu et al. 2013). The key to this analytical method is the assumption that the distribution pattern of the mudstone mechanical parameters obeys a Gaussian random distribution, including the cumulative distribution function (CDF), and its derivative form, the probability distribution function (PDF). The CDF and PDF curves for the mechanical parameters of the material (H_{IT}, E_{IT}) can be obtained from the statistics of the test data. The Gaussian distribution curve for each material can therefore be determined from the mean μ_j^M, μ_j^H and the standard deviation s_j^M, s_j^H, with μ representing the statistical value. In the following equation, N is used to represent the number of indentations in a phase, Mi and Hi are the E_{IT} and H_{IT} of each indentation test (Deirieh et al. 2012):

$$D_X\left(X_i\right) = \frac{i}{N} - \frac{1}{2N}, i \in [1, N], X = (M, H)$$

$$G_X(X_i) = 1, n, D\left(X_i; \mu_j^X, s_j^X\right)$$

$$= \frac{1}{s_j^X \sqrt{2\pi}} \times \int_{-\infty}^{X_i} exp\left(\frac{-\left(u - \mu_j^X\right)^2}{2\left(s_j^X\right)^2}\right) du, X = (M, H)$$

In the equation, it is assumed that the material contains j = 1, n phases, which can be determined by XRD experiments. $G_X(X_i)$ is a Gaussian distribution function. The proportion relative to the total area of the indentation is fj. Unknown n*5 matrix $\left\{f_j, \mu_j^M, s_j^M, \mu_j^H, s_j^H\right\}$, j = 1, n can be obtained by minimizing the difference between the PDF curve obtained by the experiment and deconvolution.

$$min \sum_{i=1}^{N} \sum_{X=(M,H)} \left(\sum_{j=1}^{n} f_j D\left(X_i; \mu_j^X, s_j^X\right) - D_X\left(X_i\right) \right)^2$$
$$\text{s.t.} \tag{7}$$
$$\sum_{j=1}^{n} f_j = 1$$

It should be emphasized that, because the PDF curve is the differential form of the CDF, once the form of the CDF curve of the material is confirmed, its PDF can also be obtained in the same way. According to experience, it is more intuitive to use PDF for deconvolution to obtain the distribution of mechanical parameters.

Upscaling models

In this paper, based on the single mineral components and their volume fractions obtained by deconvolution, together with the upscaling model, the E_{IT} of mudstone at the mesoscale was up-scaled to the macroscale. The E_{IT} of similar composition-content bulk rocks in the paper were combined to evaluate the applicability of these upscaling models to mudstones.

MT homogenization method has been widely used in scaling up by assuming k elliptical solid particles embedded in an infinite homogeneous matrix. Homogenization of granite based on the Mori–Tanaka method was carried out in two steps (Mori and Tanaka 1973). In the first step, the mechanical properties of the clay matrix consisting of illite and various types of pore fractures in the mudstone were converted to the mechanical properties of the matrix solid phase with pores on the surface:

$$k_{\mathrm{low}} = \frac{4(1-\varphi)k_{\mathrm{s}}\mu_{\mathrm{s}}}{4\mu_{\mathrm{s}} + 3\varphi k_{\mathrm{s}}} \tag{8}$$

$$\mu_{\mathrm{low}} = \frac{(1-\varphi)\mu_{\mathrm{s}}}{1 + 6\varphi \frac{k_{\mathrm{s}}+2\mu_{\mathrm{s}}}{9k_{\mathrm{s}}+8\mu_{\mathrm{s}}}} \tag{9}$$

In the second step, the mechanical properties of the clastic minerals, consisting of quartz, microcline and albite together with the matrix solid phase with pores converted in the first step, were transformed into the mechanical properties of the mudstone at the macroscopic scale.

$$K_{\mathrm{MT}}^{\mathrm{hom}} = \left(\sum_{r=1}^{3} f_r \frac{k_r}{3k_r + 4\mu_{\mathrm{low}}} \right) \left(\sum_{r=1}^{3} \frac{f_r}{3k_r + 4\mu_{\mathrm{low}}} \right)^{-1} \tag{10}$$

$$G_{\mathrm{MT}}^{\mathrm{hom}} = \frac{\sum_{r=1}^{3} \frac{f_r \mu_r}{\mu_{\mathrm{low}}(9k_{\mathrm{low}}+8\mu_{\mathrm{bw}})+6\mu_r(k_{\mathrm{low}}+2\mu_{\mathrm{low}})}}{\sum_{r=1}^{3} \frac{f_r}{\mu_{\mathrm{low}}(9k_{\mathrm{low}}+8\mu_{\mathrm{bw}})+6\mu_r(k_{\mathrm{low}}+2\mu_{\mathrm{low}})}} \tag{11}$$

where: k_{low} and μ_{low} are the bulk modulus and shear modulus of the porous matrix, respectively, and φ is the porosity of the matrix.

Kuster-Toksöz used "the long-wavelength first-order scattering theory" to propose a method for describing the mechanical properties of solids as well as inclusions in the matrix. On this basis, Berryman (1992) proposed a general expression for the KT model:

$$\left(K_{\mathrm{hom}} - K_0\right) \frac{\left(K_0 + \frac{4}{3}G_0\right)}{\left(K_{\mathrm{hom}} + \frac{4}{3}G_0\right)} = \sum_{J=1}^{k} f_J\left(K_J - K_0\right)P^{0J} \tag{12}$$

$$\left(G_{\mathrm{hom}} - G_0\right) \frac{\left(G_0 + \zeta_0\right)}{\left(G_{\mathrm{hom}} + \zeta_0\right)} = \sum_{J=1}^{k} f_J\left(G_J - G_0\right)Q^{0J} \tag{13}$$

The coefficients P and Q represent the specific shape of the particles, ζ_0 is related to the properties of the matrix, and the superscript J represents the matrix and the J-th matrix inclusion. The value method of these parameters can be found in Berryman's related paper (Berryman 1992).

The essence of DEM theory is to increase a small part of inclusions in the matrix, and gradually increase the content of inclusions to make it finally reach the actual proportion (Huang et al. 2014; Kong et al. 2019). The coupled ordinary differential equations of the model can be summarized as:

$$(1 - y)\frac{d}{dy}\left[K_{\mathrm{hom}}(y)\right] = \left(K_2 - K_{\mathrm{hom}}\right)p^J \tag{14}$$

$$(1 - y)\frac{d}{dy}\left[\mu_{\mathrm{hom}}(y)\right] = \left(\mu_2 - \mu_{\mathrm{hom}}\right)Q^J \tag{15}$$

where K_{hom} and μ_{hom} are the volume and shear modulus of the matrix, respectively, K_2 and μ_2 are the volume and shear modulus of the added inclusions, and y is the concentration of the inclusions relative to the matrix.

Results

Characteristic curve of nanoindentation test

The quartz and clay matrix parts were selected for indentation test to obtain representative quartz-dominated and clay matrix-dominated load-depth curves. It can be seen from Fig. 6 that the maximum indentation depth of quartz was much smaller than that of the clay matrix region, and its maximum indentation depth under the peak load of 3 mN was controlled within 66 nm. The maximum indentation
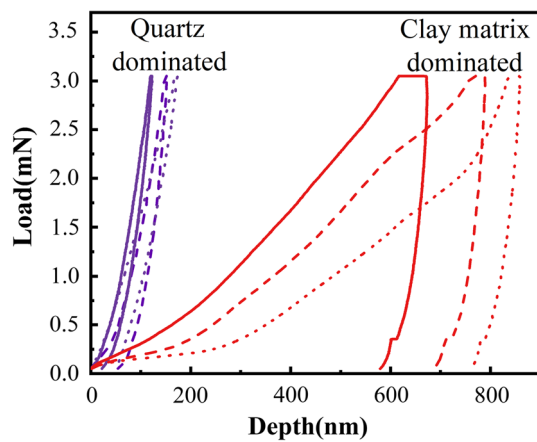
Fig. 6 Nanoindentation test results for a specific area

depths in the clay matrix region were 581, 693, and 761 nm, respectively. The quartz had a smoother loading curve and a shorter load retaining phase, which indicated a smaller amount of creep. During the unloading stage, the deformation of the quartz recovered quickly and the recovery was also greater, with less residual deformation. This indicates that the quartz has good homogeneity, stable mechanical properties and a high E_{IT} and H_{IT}. The load-indentation depth curve of the clay matrix had a high degree of dispersion. In the loading stage, the indentation depth increased rapidly, and some curves showed obvious concave-convex transitions. The residual deformation in the unloading stage was large and the plastic deformation was obvious. This

indicates that the texture of the clay matrix is soft and the mechanical properties are poor.

By substituting the relevant parameters extracted in Fig. 6 into Eqs. 1–6, the values of E_{IT} and H_{IT} of the relevant region can be obtained by calculation.

Distribution of E_{IT}

The E_{IT} distribution on the four 5*5 grid areas, which was calculated according to Eqs. 1–6 was reflected in the cloud map shown in Fig. 7. The E_{IT} distribution reflected in the figure showed that the mudstone surface was highly inhomogeneous. With reference to previous preliminary estimates of E_{IT} for the three minerals contained in this mudstone, quartz, feldspar and illite (Du et al., 2022). The E_{IT} magnitude of quartz is above 100 GPa, 45–85 GPa for feldspar minerals, while the E_{IT} of clay matrix is generally below 45 GPa. Further analysis showed that the three minerals in the mudstone samples were uniformly distributed, and the quartz and feldspar were mainly connected by clay matrix, which was similar to the phenomenon reflected in Fig. 2. It is noteworthy that the E_{IT} distribution around some of the indentation sites shows the interlocking characteristics of multiple mineral compositions. This is because this part of the indentation point is located at the interface between the clay matrix and the feldspar and quartz. As a result, the clay matrix is overlaid on the mineral particles to form a film-like material structure. When the indentation depth is large, the elastic/plastic zone at the tip of the indenter affects the mineral particles

Fig. 7 Cloud map of the distribution of E_{IT}
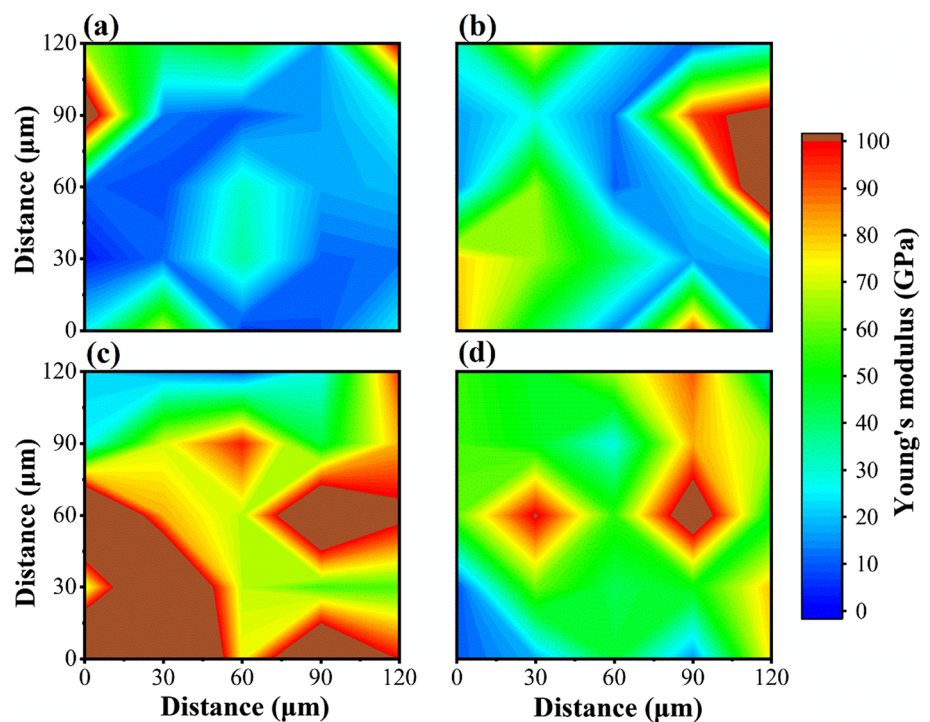
to produce a 'base effect' (Li et al., 2021). In this case, as the indentation depth increases, the zone of elastic–plastic deformation produced by the indentation increases and the mechanical response gradually transition from a mechanical response dominated by quartz particles to clay matrix.

In addition, according to the XRD test results in Table 1, the most abundant mineral composition in the sample is quartz (53.8%), but obviously the E_{IT} distribution obtained by this nanoindentation test does not conform to this conclusion. This is due to the fact that the clay matrix contains the pore and fracture structures in the surface. The test results of nanoindentation reflect the volume fraction occupied by each mineral component on the surface of the sample, in its original condition. The XRD test, on the other hand, cannot accurately characterize the pore and fracture distribution on the sample surface because of the grinding of the sample before the test.

Relationship between mudstone H_{IT} and E_{IT}

The overall distribution of mudstone H_{IT} and E_{IT} is shown in Fig. 8a. Among them, the number of indentation points located in the region with E_{IT} less than 50GPa is the largest. Generally speaking, the mechanical properties vary greatly depending on the mineral composition of the indentation, but the graph shows a good continuity in the distribution of

Fig. 8 Relationship between mudstone H_{IT} and E_{IT}

(a) Overall distribution of H_{IT} and E_{IT}

(b) Linear fitting relationship between H_{IT} and E_{IT} on four regions
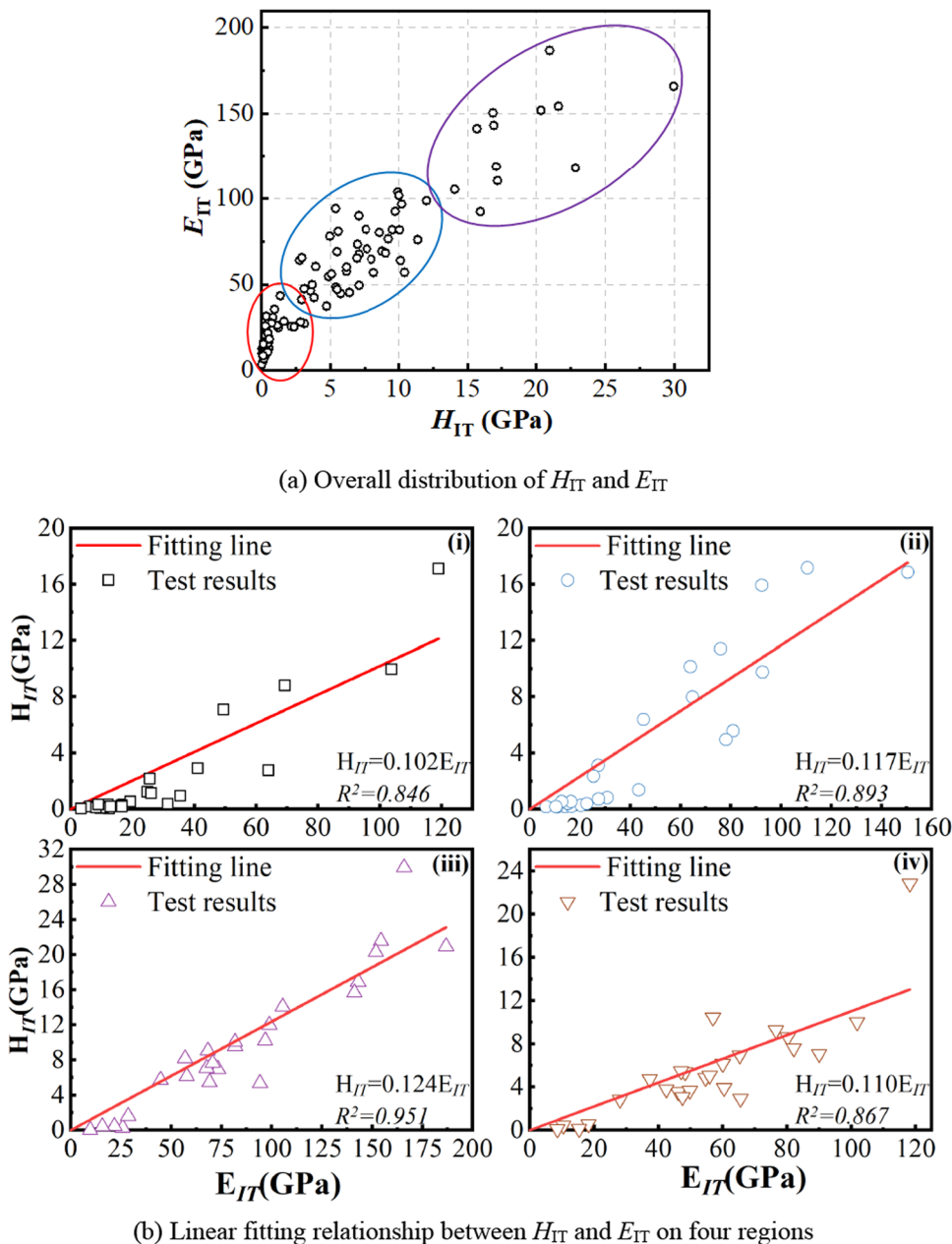
E_{IT} and H_{IT}. This also shows that part of the indentation acts on the interface region of the two mineral compositions, and at the same time characterizes the comprehensive mechanical properties of the multiphase composition.

In Fig. 8b, the H_{IT} and E_{IT} of the selected four regions were linearly fitted. The equation of $H_{IT} = k_1 E_{IT}$ was used for linearly fitting, where k_1 corresponded to the slope in the fitting equation, the slopes of the four regions were 0.102, 0.117, 0.124, 0.110, respectively, and the optimization degrees of fitting were 0.846, 0.893, 0.951, 0.867 respectively. Unlike the previous general linear relationship (Kong et al. 2019), H_{IT} increases linearly with increasing modulus of elasticity, with an intercept of 0. In addition, as the optimality of the fit remains highly stable for different regions, it shows that the relationship between H_{IT} and E_{IT} is not influenced by parameters such as mineral composition and depth of deformation, but is a self-contained property of the material itself. Based on this property, the characterization of the mechanical properties of the mudstone can be carried out in subsequent studies using E_{IT} as a proxy.

Deconvolution analysis

The right bin size can control the details of a random variable distribution between too much (under-smoothing) and too little (over-smoothing). In short, it means that a larger bin size helps to achieve a noise-reducing treatment of the randomness distribution, while a smaller bin size captures the distribution properties more precisely (Wand 1997). This deconvolution analysis was carried out using two separate sets of bin sizes. The sample compositions of the XRD test results were characterized and the clay matrix-quartz and clay matrix-feldspar mineral interfaces were considered, respectively. Albite and Microcline can be collectively referred to as feldspar minerals in the process of deconvolution, because Albite and Microcline are both feldspar minerals, and their mechanical properties are relatively close.

The bar at the bottom of Fig. 9a corresponds to the E_{IT} distribution of the mudstone at different bin sizes, and the curves are the E_{IT} of each mineral composition in the mudstone after PDF deconvolution by Eq. 7. Figure 8a also gives a comparison between the cumulative peak fit curve obtained by deconvolution and the PDF distribution curve obtained from the nanoindentation test. It can be found that the fitting degree between the sample curves before and after immersion was good, which also shown that this data analysis method can be used to characterize the E_{IT} distribution of each composition of mudstone. Then, the bin size was appropriately reduced, and the distribution characteristics of the indentation points located in the two interface regions are described in detail, as shown in Fig. 8b. The 1st and 2nd interfaces in the figure represent two interfaces of clay
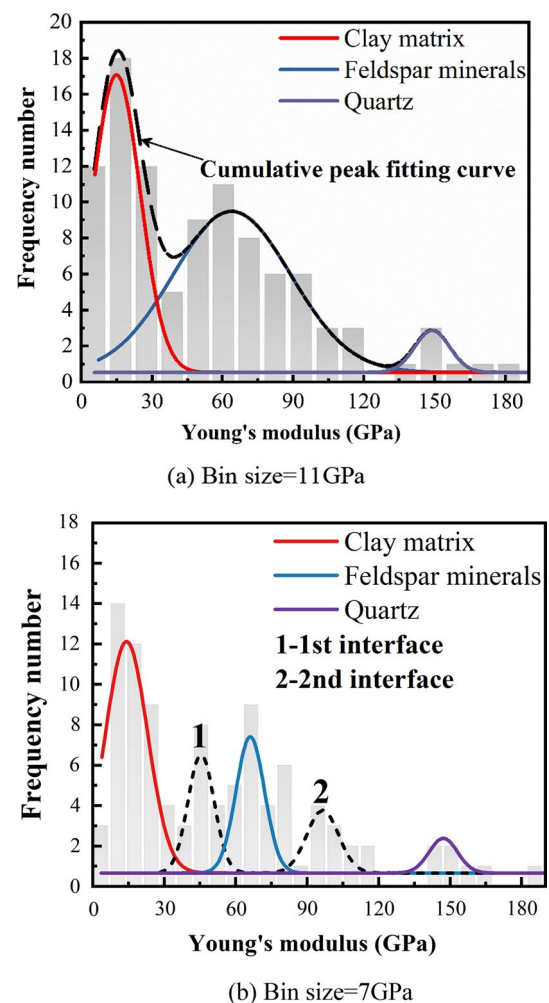

(a) Bin size=11GPa

(b) Bin size=7GPa

Fig. 9 Deconvolution result of PDF

matrix-quartz and clay matrix-feldspar minerals, respectively. The deconvolution results of mudstone E_{IT} under two bin sizes were listed in the following table.

Combining Fig. 9 and Table 2, it can be found that different bin sizes have little effect on the values of E_{IT} of the three mineral compositions. When bin size is 11 GPa, the E_{IT} of clay minerals, feldspar-like minerals and quartz are 16.1, 64.84 and 149.69 GPa respectively, which are close to the results reported in the papers (Yin and Hu 2004). Comparing the deconvolution results under the two bin sizes, the number of indentations from clay matrix and feldspar minerals was significantly reduced. For larger bin size, the number of indentation points belonging to the interfacial region was accounted for in the component with the relatively low E_{IT}, and because the number of indentations in this part is relatively small, no new peaks were formed. The E_{IT} of the two groups of interfaces are 43.34 and 97.01GPa, respectively. When the indenter was

Table 2 E_{IT} obtained by deconvolution

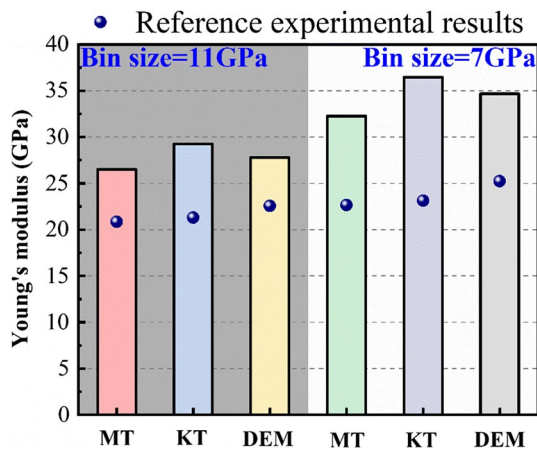| E_{IT}/GPa	Clay matrix	1st interface	Feldspar minerals	2nd interface	Quartz
Bin size = 11	16.1	–	64.84	–	149.69
Bin size = 7	14.61	46.34	66.3	97.01	148.37

Fig. 10 Comparison of E_{IT} obtained by upscaling models and experimental results

pressed into the clay matrix and mineral particles were present near the indenter tip, the clay matrix can be used as the membrane material and the mineral particles as the base material to form a clay matrix/quartz-like particle composition. In this case, as the indentation depth increases, the mechanical response will gradually transition from the dominance of clay matrix to that of quartz particles (Xu et al. 2021). Similarly, when the indenter pressed into the quartz particles and clay matrix was present near the indenter tip, the quartz particles could be used as the membrane material and the clay matrix as the base material, forming a quartz-like particles/clay matrix composition. In this case, as the indentation depth increased, the mechanical response gradually transited from dominated by quartz particles to dominated by clay matrix.

Validation and optimization of the upscaling models

Model validation

Figure 10 and Table 3 show the E_{IT} of each composition obtained under two bin sizes, and the results after processing by the upscaling models (MT, KT, DEM). In the case of known deconvolution results, the indentation frequency corresponding to each mineral composition was compared with the total indentation frequency to obtain the volume fraction of the corresponding compositions. The parameters such as E_{IT} and volume fraction of each mineral composition were also substituted into the model, so that the mechanical properties of the mudstone obtained by nanoindentation can be scaled up and studied. The essence of the upscaling model is a homogenization method, which homogenizes the mechanical properties at the mesoscopic scale to obtain the mechanical properties at the macroscopic scale. In this paper, the E_{IT} values for rocks with similar mineral composition content to the mudstone used in this study were obtained by searching the relevant papers. When the bin size was 7 GPa, the scaling process needed to consider the volume fractions of the two interfaces and their corresponding E_{IT}. At this point the E_{IT} values increased further, to 32.25, 36.47 and 34.69 GPa respectively. As we have analyzed previously, decreasing the bin size caused the otherwise ineffective high E_{IT} distribution in the mineral composition to peak separately, thus further increasing the overall E_{IT} of the sample. According to the analysis in Table 3, it can be seen that there was a large error with the macroscopic E_{IT} obtained by the three scale-up models. It is shown that the scaled E_{IT} was greater than the results of traditional mechanical tests, and the average error rate of the whole can reach 41.23%. A large number

Table 3 Error analysis of E_{IT} obtained by upscaling models

Method	Young's modulus (Gpa)	Reference value (GPa)					
		(Xu et al. 2021)				(Yin and Hu 2004)	(Magnenet et al. 2011)
		18.24	18.64	19.74	19.83	22.08	20.25
		Error (%)					
Mori–Tanaka	26.51	45.34	42.22	34.30	33.69	20.06	30.91
Kuster-Toksöz	29.26	60.42	56.97	48.23	47.55	32.52	44.49
DEM	27.79	52.36	49.09	40.78	40.14	25.86	37.23
Mean value	27.85	41.23					

of studies have shown that the macroscopic E_{IT} obtained by upscaling models is too large (Xu et al. 2021; Yin and Hu 2004; Magnenet et al. 2011), which seriously affected the scope and accuracy of this type of homogenization model.

Analysis of the reasons for such errors can be divided into two categories. The first category is due to the limitations of the model itself. Taking the MT model as an example, there are three main limitations. (1) This model is only applicable to composites with a small volume fraction of inclusion phase. In this study, the clay matrix was taken as the matrix phase, and the quartz and feldspar minerals were used as the inclusion phase. (2) The MT model assumes that the structure of the material is homogeneous, and neglects the influence of the size and number of impurity phases. (3) The model is based on the Eshelby tensor (Eshelby 1957) assuming that the shape of the impurity phase is elliptical. According to the microstructure of mudstone in Fig. 2, the surface structure and shape of impurity phase are highly heterogeneous. The KT model is a method suitable for describing the mechanical properties of solids and encapsulated matrices, which also makes idealized assumptions about the shape of the encapsulated solid. DEM model is only available for three-phase composites. However, in this study, the deconvoluted dataset actually has 4–6 different phases. In order to be able to use the DEM model for analysis, the deconvolution results need to be pre-processed. For example, when processing the deconvolution model with bin size = 7, quartz and feldspar were pre-converted into a unified virtual phase whose E_{IT} magnitude was equal to the weighted average of the two compositions. These antecedent steps may affect the accuracy of the use of the upscaling model. In addition to this, the DEM model is also affected by the highly non-homogeneous nature of the mudstone. The second category of reasons for the error is mainly due to local damage to the rock as a result of loading tests at the macro scale. Charlton et al. (2021) applied the MT method to homogenize the macroscopic modulus of elasticity of shale and found that the results of the ascending scale tended to be larger than those of triaxial compression tests. It was also suggested that this may be caused by local damage to the rock during loading. These damages mainly occur in the interface area of each mineral composition, because the mechanical properties of the mineral interface are generally weaker than that of the mineral itself, and a weak interlayer with a certain thickness is formed at the mesoscale.

Optimization of the upscaling models

The relationship between the equivalent E_{IT} after scaling up and the volume fraction of the clay matrix is shown in Fig. 11. As can be seen from Fig. 10, all three upscaling models are very sensitive to the volume fraction of the contained clay matrix, and the interrelationships are roughly of
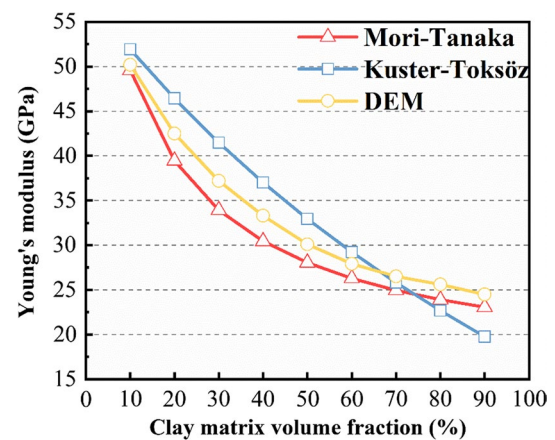

Fig. 11 Relationship between volume fraction of clay matrix and E_{IT}

the form of an inverse proportional function. The optimization method proposed in this paper focuses on addressing the second category of causes for errors. By adjusting the volume percentage of the clay matrix, the E_{IT} of the mudstone interface area is closer to the condition of the macro loading test.

As already analyzed above, damage to mudstones during macroscopic loading occurs mainly in the interface region of the mineral composition. For the mineral compositions in this study, they are clay matrix-quartz interface and clay matrix-feldspar minerals' interfaces. Figure 11 shows the microstructure changes of mudstone before and after macro loading. The external manifestation of the damage occurring in the interface area is the increase in tiny pores and cracks, as shown in Fig. 12c, d. Compared with the original condition (Fig. 12a, b), a large number of through cracks appeared at the junction of solid particles, and the width of the cracks expanded from generally no more than 5 µm to several tens of microns. Even some clastic minerals were separated from the mineral framework, which leads to the increase of clay matrix area.

In this case, the E_{IT} in the interface region is no longer a weighted average of the two mineral compositions or a value somewhere in between, but more inclined to the E_{IT} of the clay matrix. It is obvious that the E_{IT} and its volume fraction in the interface area in Table 2 do not conform to the actual situation. Therefore, we uniformly set the E_{IT} of the two interface regions as the value of the clay matrix under the same conditions. This indirectly increases the volume fraction of the clay matrix in the scale-up process, which has the effect of reducing the equivalent E_{IT} and the error between it and the mechanical properties obtained from the macroscopic tests. The optimized equivalent E_{IT} magnitudes and the corresponding error statistics are shown in Fig. 13 and Table 4. The magnitudes of the E_{IT} values for the three upscaling models were optimized and reduced to 20.53,

Fig. 12 Changes of mudstone surface structure before and after macro loading, **a**, **b** are the original sample surface before loading test, **c**, **d** are the sample surface after loading failure
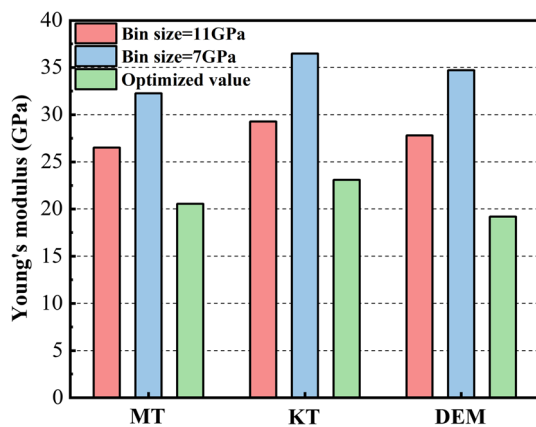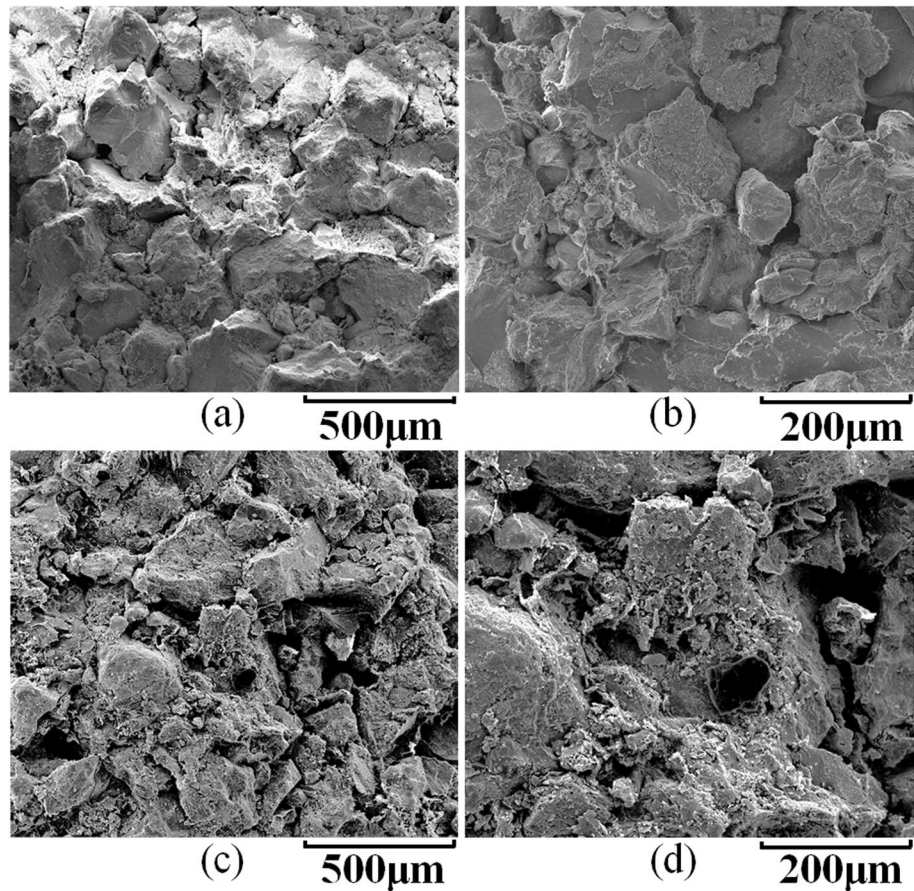

Fig. 13 Comparison of E_{IT} obtained by upscaling before and after optimization

23.09 and 19.17 GPa, respectively, and the error between them and the reference value was reduced from the original 41.23% to 10.14%. It is shown that this optimization method can better modify the upscaling model. And make the condition and E_{IT} of the interfacial region closer to the real situation under macroscopic loading tests.

To further validate the feasibility of this optimization method, it was also used to revise the upscaling model of materials in other studies. The optimized results are shown in Table 5. Due to the limitation of upscaling models used in other studies, this paper can only modify the models used in it. In addition, for studies that do not give values for the modulus of elasticity in the interfaces as well as the volume fraction (Li et al. 2021; Da Silva et al. 2013; Zhang et al. 2021; Liu et al. 2022; Shi et al. 2019; Li et al. 2022; Zhang et al. 2018a, b), the E_{IT} and errors for these materials after upscaling were also listed. It can be seen that the scaled-up E_{IT} of the above materials was greater than the experimental results, with error rates generally higher than 10%. For sandstone (Li et al. 2021), the error between the E_{IT} obtained by upscaling and the experiment was more than 49.4%. Then, the optimization method was used, the value of E_{IT} in the interface was set to 3.11 GPa of clay matrix, and the corresponding volume fraction was substituted. After optimization, the error of E_{IT} obtained by using upscaling models decreased to less than 26.2%. For Conglomerate (Zhang et al. 2022) and Kaolinite (Liu et al. 2022), the optimization method has also achieved good results, and the error has decreased by 16.7–57.8%. It should be emphasized that

Table 4 Error analysis of E_{IT} obtained by upscaling models after optimization

Method	Optimized value	Error (%)					
		(Xu et al. 2021)				(Yin and Hu 2004)	(Magnenet et al. 2011)
Mori–Tanaka	20.53	12.55	10.14	10.14	3.53	7.55	1.38
Kuster–Toksöz	23.09	26.59	23.87	16.97	16.44	4.57	14.02
DEM	19.17	5.1	2.84	2.89	3.33	15.18	5.33
Mean value	20.93	10.14					

the optimization effect is related to the volume fraction corresponding to the interface area. In general, the higher the degree of internal heterogeneity of the material, the more kinds of mineral compositions it contains, the better the optimization effect will be. In addition, for various materials with different mineral compositions, the choice of matrix phase and inclusion phase is also an important factor affecting the results of scaling and optimization.

Discussion

Nanoindentation technology has great advantages in characterizing the micromechanical properties of geotechnical materials (Sun et al. 2020). However, without the assistance of data analysis methods, the test results can only characterize the overall E_{IT} or H_{IT} distribution within a microscopic region. The application of deconvolution method can further divide the test results of nanoindentation, making it easy to obtain mechanical characteristics at the mineral composition scale. Bin size is an important factor that affects the results of deconvolution (Du et al. 2022). In this paper, when bin size = 11 GPa, and the number of peaks is consistent with the number of mineral compositions obtained by XRD testing, which indicates that the deconvolution results under this bin size can more accurately characterize the E_{IT} values of the

three mineral components. When an indentation is applied to the interfaces of multiple mineral compositions, it characterizes the mechanical properties of the composite of these mineral compositions. By selecting a smaller bin size, more details about the PDF distribution on the interfaces can be obtained. In addition, PDF deconvolution can also reflect the volume fraction of mineral compositions.

Based on the volume fraction and E_{IT} of each mineral composition obtained from the nanoindentation test, upscaling models such as MT, KT, and DEM can be used to obtain mechanical property parameters at the macro scale. Compared with the results of indoor experiments, the mechanical parameters obtained using upscaling models are generally larger. In order to reduce this error, this study proposed that E_{IT} of the interface region can be set to the value of the E_{IT} of clay matrix under equivalent conditions. Because this can more accurately characterize the actual situation of the mineral compositions interface region under macro loading tests. The measurement of E_{IT} in the interface region of various mineral compositions requires further study. On the one hand, the number of indentations can be further increased to obtain more details of PDF. Whether there is a certain correlation between the number of indentations and the final deconvolution results has not been systematically studied. On the other hand, in the future, nanoindentation test can be performed on selected interface regions and associated

Table 5 Error analysis of optimized upscaling models of other materials

Material type	E_{IT} (GPa) (error,%)			E_{IT} (GPa)* (error,%)*		
	MT	KT	DEM	MT	KT	DEM
Sandstone	68.5 (51.9)	67.6 (49.9)	67.4 (49.4)	56.9 (26.2)	55.6 (23.3)	54.8 (20.8)
Concrete	40.7 (16.6)	–	–	–	–	–
Conglomerate	17.69 ~ 30.44 (21 ~ 116)	–	–	13.71 ~ 26.96 (17.5 ~ 83.2)	–	–
Kaolinite	–	–	3.25 (10.2)	–	–	3.19 (7.5)
Shale	41.12, 39.15 (9.9), (11.4)	–	–	–	–	–
Granite	62.63 (> 4.1)[b]	–	–	–	–	–
Claystone	5.62 (11.1)	–	–	–	–	–

*The E_{IT} in this part is the value obtained by using the optimization method proposed in this paper and the error between the experimental results. b: The indoor experiments in this group were carried out under confining pressure of 5 MPa and the experimental results obtained would be biased to a greater extent, which would result in a smaller error

mineral compositions. This will allow a more in-depth analysis of the relationship between the indentation location and the obtained E_{IT} of the interface. In addition, this study only focuses on the mudstone in Southern China. In subsequent researches, other engineering materials can be used to expand the application scope of the upscaling models and the optimization methods proposed in this paper.

Conclusions

In this paper, the mechanical property of mudstone at the mesoscale was analyzed using nanoindentation technology combined with the deconvolution method. The homogenization and upscaling models were also adopted to realize the evaluation of the mechanical properties of mudstone. The main conclusions obtained are as follows:

1. Through SEM–EDS and XRD methods, mudstone can be considered as a highly heterogeneous multiphase material. Illite and various pores and cracks formed the clay matrix, and quartz and feldspar minerals formed the grain skeleton.
2. The H_{IT} and E_{IT} of each position and mineral composition satisfy a linear relationship. The mechanical response of the mineral compositions in the interfacial region is complex, mainly responding to the composite mechanical properties of the clay matrix and different clastic minerals. Such a characteristic made the overall mechanical properties of the mudstone show good continuity in the nanoindentation test.
3. The deconvolution method can accurately obtain the mechanical properties of each mineral composition in the mudstone. The E_{IT} for the clay matrix, feldspar minerals and quartz in the mudstone is 16.1, 64.84, and 149.69 GPa, respectively. The E_{IT} of the interface regions can be obtained by reducing the bin size, which is 148.37 and 46.34 GPa for the clay matrix-quartz and clay matrix-feldspar minerals, respectively.
4. The Young's modulus values calculated by upscaling models are larger than those obtained from macro tests. According to the actual situation of the interface region under macro loading test, the E_{IT} of the interface region should be set to the value of the E_{IT} of the clay matrix. This method can effectively improve the model. Based on the results of this study, the error is reduced from 41.23 to 10.14%.

Declarations

Conflict of interest The authors declare that they have no known competing financial interests or personal relationships that could have appeared to influence the work reported in this paper.

References

Berryman JG (1992) Single-scattering approximations for coefficients in Biot's equations of poroelasticity. J Acoust Soc Am 91:551–571. https://doi.org/10.1121/1.402518

Charlton S, Goodarzi M, Rouainia M et al (2021) Effect of diagenesis on geomechanical properties of organic-rich calcareous shale: a multiscale investigation. J Geophys Res-Sol Ea 126:1–23. https://doi.org/10.1029/2020JB021365

Constantinides G, Chandran KSR, Ulm FJ, Van Vliet KJ (2006) Grid indentation analysis of composite microstructure and mechanics: principles and validation. Mat Sci Eng a-Struct 430:189–202. https://doi.org/10.1016/j.msea.2006.05.125

Corkum AG, Martin CD (2007) The mechanical behaviour of weak mudstone (Opalinus Clay) at low stresses. Int J Rock Mech Min 44:196–209. https://doi.org/10.1016/j.ijrmms.2006.06.004

Da Silva WRL, Nemecek J, Štemberk P (2013) Application of multi-scale elastic homogenization based on nanoindentation for high performance concrete. Adv Eng Softw 62:109–118. https://doi.org/10.1016/j.advengsoft.2013.04.007

Davydov D, Jir´asek, M., Kopecký, L., (2010) Critical aspects of nano-indentation technique in application to hardened cement paste. Cement Concr Res 41:20–29. https://doi.org/10.1016/j.cemconres.2010.09.001

Deirieh A, Ortega JA, Ulm F, Abousleiman YN (2012) Nanochemo-mechanical assessment of shale: a coupled WDS-indentation analysis. Acta Geotech 7:271–295. https://doi.org/10.1007/s11440-012-0185-4

Doebelin N, Kleeberg R (2015) Profex: a graphical user interface for the Rietveld refinement program BGMN. J Appl Crystallogr 48:1573–1580. https://doi.org/10.1107/S1600576715014685

Du JT, Luo SM, Hu LM et al (2021) Multiscale mechanical properties of shales: grid nanoindentation and statistical analytics. Acta Geotech 17:339–354. https://doi.org/10.1007/s11440-021-01312-8

Eshelby JD (1957) The determination of the elastic field of an ellipsoidal inclusion, and related problems. Proc R Soc London Ser A Math Phys Sci 241(1226):376–396. https://doi.org/10.1098/rspa.1957.0133

Hu, M., Xu, G.Y., Hu, S.B., et al., 2013. Study of equivalent elastic modulus of sand gravel soil with Eshelby tensor and Mori-Tanaka equivalent method. Rock Soil Mech, 34, 1437–1448. (in Chinese). https://doi.org/10.16285/j.rsm.2013.05.017.

Huang Y, Shen WQ, Shao JF et al (2014) Multi-scale modeling of time-dependent behavior of claystones with a viscoplastic compressible

porous matrix. Mech Mater 79:25–34. https://doi.org/10.1016/j.mechmat.2014.08.003

Kang X., Hu W.X., Wang J., Cao J., Zhao Y., 2017. Fan-delta sandy sandy conglomerate reservoir: sensitmty: A case study of the Baikouquan formation in the Mahu sag, Junggar basin. Journal of China University of Mining & Technology. 46, 596–605. https://doi.org/10.13247/j.cnki.jcumt.000607.

Kong LW, Zeng ZX, Bai W, Wang M (2018) Engineering geological properties of weathered swelling mudstones and their effects on the landslides occurrence in the Yanji section of the Jilin-Hunchun high-speed railway. Bull Eng Geol Environ 77:1491–1503. https://doi.org/10.1007/s10064-017-1096-2

Kong L, Ostadhassan M, Zamiran S, Liu B, Li C, Marino GG (2019) Geomechanical Upscaling Methods: Comparison and Verification via 3D Printing. Energies 12:382. https://doi.org/10.3390/en12030382

Kuster GT, Toksöz MN (1974) Velocity and attenuation of seismic waves in two-phase media: Part I. theoretical formulations. Geophysics 39:587–737. https://doi.org/10.1190/1.1440450

Li C, Zhang FH, Wang X, Rao XS (2018) Investigation on surface/subsurface deformation mechanism and mechanical properties of GGG single crystal induced by nanoindentation. Appl Optics 57:3661–3668

Li, Y., Luo, S. M., et al., 2021. Cross-scale characterization of sandstones via statistical nanoindentation: Evaluation of data analytics and upscaling models. Int J Rock Mech Min, 142, 104738. https://doi.org/10.1016/j.ijrmms.2021.104738.

Li, M.Y., Peng, L., Zuo, Z.P., et al. 2022. Study on multi-scale mechanical properties of granite based on DIP-FFT numerical method. 41(11), 2254–2267. https://doi.org/10.13722/j.cnki.jrme.2022.0029.

Liu L, Li YC, Wu YK et al (2022) Strengthening mechanisms in cement-stabilized kaolinite revealed by cross-scale nanoindentation. Acta Geotech 17:5113–5132. https://doi.org/10.1007/s11440-022-01493-w

Luo TY, Zhang QS, Liu ZB et al (2022) Nanoindentation experimental study on mechanical properties of red mudstone in Hechi, Guangxi Province. Journal of Water Resources & Water Engineering 33:174–181 (**(in Chinese)**)

Ma ZY, Gamage RP, Zhang CP (2020) Application of nanoindentation technology in rocks: a review. Geomech Geophys Geo 6:1–27. https://doi.org/10.1007/s40948-020-00178-6

Magnenet V, Auvray C, Francius G, Giraud A (2011) Determination of the matrix indentation modulus of Meuse/Haute-Marne argillite. Appl Clay Sci 52:266–269. https://doi.org/10.1016/j.clay.2011.03.001

Miller M, Bobko C, Vandamme M, Ulm FJ (2007) Surface roughness criteria for cement Paste nanoindentation. Cement Concr Res 38:467–476. https://doi.org/10.1016/j.cemconres.2007.11.014

Mori T, Tanaka K (1973) Average stress in matrix and average elastic energy of materials with misfitting inclusions. Acta Metall 21:571–574. https://doi.org/10.1016/0001-6160(73)90064-3

Němeček J (2009) Creep effects in nanoindentation of hydrated phases of cement pastes. Mater Charact 60:1028–1034. https://doi.org/10.1016/j.matchar.2009.04.008

Oliver WC, Pharr GM (1992) An improved technique for determining hardness and elastic modulus using load and displacement sensing indentation experiments. J Mater Res 7:1564–1583. https://doi.org/10.1557/JMR.1992.1564

Oliver WC, Pharr GM (2004) Measurement of hardness and elastic modulus by instrumented indentation: Advances in understanding and refinements to methodology. J Mater Res 19:3–20. https://doi.org/10.1557/jmr.2004.19.1.3

Oliver WC, Pharr GM (2011) Measurement of hardness and elastic modulus by instrumented indentation: advances in understanding and refinements to methodology. J Mater Res 19:3–20. https://doi.org/10.1557/jmr.2004.19.1.3

Perras, M.A., Wannenmacher, H., Diederichs, M.S., 2015. Underground Excavation Behaviour of the Queenston Formation: Tunnel Back Analysis for Application to Shaft Damage Dimension Prediction. Rock Mech Rock Eng. 48, 1647–71. https://https://doi.org/10.1007/s00603-014-0656-z.

Sheng P (1990) Effective-medium theory of sedimentary rocks. Phys Rev B 41:4507. https://doi.org/10.1103/PhysRevB.41.4507

Shi, X., Jiang, S., Lu, S.F., et al., 2019. Investigation of mechanical properties of bedded shale by nanoindentation tests: A case study on Lower Silurian Longmaxi Formation of Youyang area in southeast Chongqing, China. Pet Explor Dev. 46(1), 155–164. https://doi.org/10.11698/PED.2019.01.16.

Sun CL, Li G, Gomah ME et al (2021) Experimental investigation on the nanoindentation viscoelastic constitutive model of quartz and kaolinite in mudstone. Int J Coal Sci Technol 8:925–937. https://doi.org/10.1007/s40789-020-00393-2

Sun CL, Li GC, Gomah ME, Xu JH, Rong HY (2020) Meso-scale mechanical properties of mudstone investigated by nanoindentation. Eng Fract Mech. 238:107245. https://doi.org/10.1016/j.engfracmech.2020.107245.

Ulm FJ, Vandamme M, Bobko C et al (2007) Statistical Indentation Techniques for Hydrated Nanocomposites: Concrete, Bone, and Shale. J Am Ceram Soc 90:2677–2692. https://doi.org/10.1111/j.1551-2916.2007.02012.x

Wand MP (1997) Data-based choice of histogram bin width. Am Stat 51:59–64. https://doi.org/10.1080/00031305.1997.10473591

Wu, J., Liu, S.Y., Deng, Y.F., et al., 2022. Microscopic phase identification of cement-stabilized clay by nanoindentation and statistical analytics. Appl Clay Sci. 224, 106531. https://doi.org/10.1016/j.clay.2022.106531.

Xu, D.P., Liu, X.Y., Xu, H.S., et al., 2021. Meso-mechanical properties of deep granite using nanoindentation test and homogenization approach. J Cent South Univ. 52, 2762–2771. https://doi.org/10.11817/j.issn.1672-7207.2021.08.022.

Yin YP, Hu RL (2004) Engineering geological characteristics of purplish-red mudstone of middle tertiary formation at the three gorges reservoir. J Eng Geol 12:124–135 (**(in Chinese)**)

Zhang ZH, Liu W, Han L, Chen XC, Cui Q, Yao HY et al (2018a) Disintegration behavior of strongly weathered purple mudstone in drawdown area of three gorges reservoir. China Geomorphol 315:68–79. https://doi.org/10.1016/j.geomorph.2018.05.008

Zhang F, Guo HQ, Hu DW, Shao JF (2018b) Characterization of the mechanical properties of a claystone by nano-indentation and homogenization. Acta Geotech 13:1395–1404. https://doi.org/10.1007/s11440-018-0691-0

Zhang, Z.P., Zhang, S.C., Shi, S.Z., et al., 2022. Evaluation of multi-scale mechanical properties of conglomerate using nanoindentation and homogenization methods: A case study on tight conglomerate reservoirs in southern slope of Mahu sag. Chinese Journal of rock mechanics and engineering. 41(5), 926–940. https://doi.org/10.13722/j.cnki.jrme.2021.1186.

Zhu W, Hughes JJ, Bicanic N, Pearce CJ (2007) Nanoindentation mapping of mechanical properties of cement paste and natural rocks. Mater Char 58:1189–1198. https://doi.org/10.1016/j.matchar.2007.05.018